Tunneling Spectroscopy and Inverse Photoemission: Image and Field States

G. Binnig, K. H. Frank, H. Fuchs, N. Garcia, B. Reihl, H. Rohrer, F. Salvan, and A. R. Williams
IBM Zurich Research Laboratory, 8803 Rüschlikon, Switzerland
(Received 22 April 1985)

Tunneling spectroscopy performed with the scanning tunneling microscope is used to study image-type surface states. The tunneling tip causes a Stark shift and expansion of the hydrogenic image-state spectrum, permitting a clear resolution of the individual states. A simple theoretical model provides a quantitative connection between the tunneling data and both previous and new inverse-photoemission data.

PACS numbers: 73.20.Cw, 68.20.+t, 73.40.Gk, 79.60.Cn

Image states are an interesting set of surface states, which have attracted a great deal of attention in recent years.[1-6] These hydrogenlike states are bound to a surface by the response of the substrate to the presence of the electron, and kept outside the surface by the reflective properties of the substrate. A theoretical model in which electronic motion along and perpendicular to the surface is taken to be independent yields the following relation for the binding energy of each member of the hydrogenic series:

$$E_n = \epsilon_n + E_{n,\mathrm{corr}} + (\hbar^2/2m_n^*)k_{\parallel}^2, \quad (1)$$

where n is the principal quantum number, ϵ_n is the purely hydrogenic component of the binding energy, $\mathbf{k}_{\parallel}$ is the wave vector parallel to the surface, m_n^* is the effective mass, and $E_{n,\mathrm{corr}}$ is the shift of the bottom of the band caused by deviations from perfectly free-electron motion along the surface. These states have been previously observed by LEED[2] and by k-resolved inverse-photoemission spectroscopy (KRIPES).[3-7] Also, the important role played by the image potential in the vacuum tunnel current has recently been pointed out.[7]

For image states, the electric field characterizing a tunnel junction has the effect of causing a Stark shift in the states of the hydrogenic spectrum. The evolution of the spectrum due first to corrugation effects and then to the electric field is shown in Fig. 1. The Stark shift has the effect of continuously shifting and expanding the image-state spectrum, with its accumulation of states at the vacuum level E_{vac}, into the geometric resonance spectrum associated with the V-shaped potential created by the substrate and the field. Such geometric resonances were considered by Jason[8] to explain oscillations in field ionization, and by Gundlach,[9] who predicted oscillating tunneling I-V characteristics, which were observed experimentally in semiconductor planar tunnel junctions[10] and metal-metal interfaces[11] as well as on Au tips in vacuum tunneling.[12]

The tunneling measurements we describe add the scanning capability of the scanning tunneling microscope (STM)[13,14] to the well-established capabilities of traditional tunneling spectroscopy. The benefits of this addition are numerious, e.g., bare surfaces become accessible to the full arsenal of UHV surface treatments and analysis, and it becomes possible to select and probe a suitable small portion of the surface.

Figure 2 illustrates representative tunneling spectra for several surfaces. They were taken with a voltage modulation of $\Delta V = 0.2$ V at $\nu = 200$ to 400 Hz, a frequency above the response of the feedback system

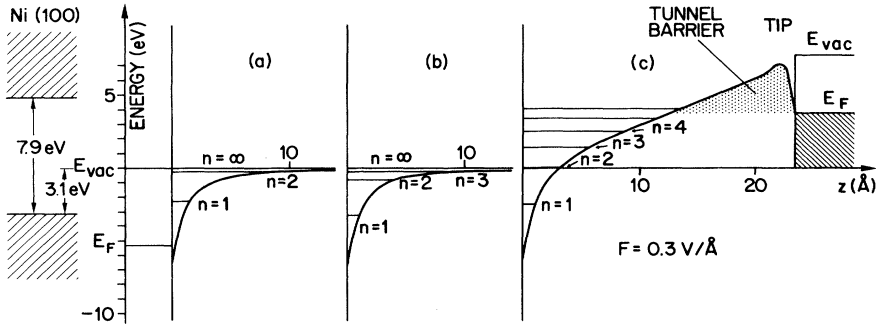

FIG. 1. Energy diagram for the electrostatic potential (including image) at a metal surface. On the left, the projected bulk band structure of the Ni(100) surface is shown shaded. Note the 7.1-eV band gap straddling the vacuum level $E_{\mathrm{vac}} = 0$. (a) For simplicity, only the $n = 1$ and $n = 2$ hydrogenic (quantum defect) energy levels are shown. (b) The surface corrugation affects the electronic x,y movement pulling the levels down, as seen by inverse photoemission. (c) Expansion and shift of the image-state spectrum by an applied field, F. The heavy solid line is the crystal potential plus the field potential.

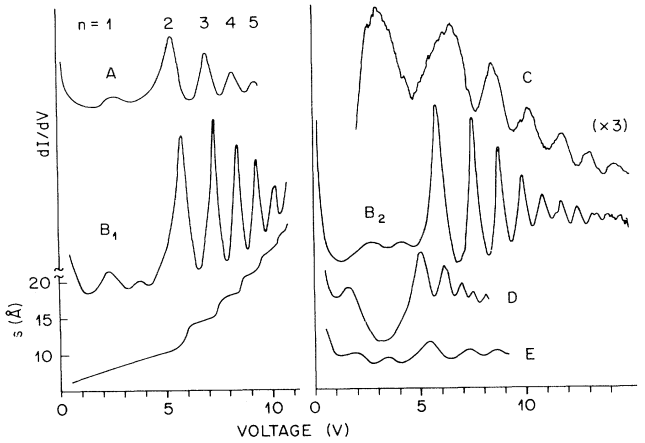

FIG. 2. Tunneling spectra dI/dV vs V for (A) clean Ni(100) surface; (B_1, low field), and (B_2, high field) oxygen-covered $c(2\times2)$ Ni(100); (C) disordered, low oxygen coverage Ni(100); (D) $(\sqrt{3}\times\sqrt{3})$ Au on Si(111); (E) Si(111)-(7×7). The voltage is scanned at constant tunnel current; the corresponding increase of the tunnel gap width is shown for B. For curve A, we have given the assignment of the peaks to the hydrogeniclike levels. The senstivity for curve C is enhanced by a factor of 3. On the $c(2\times2)$ surfaces, a small satellite peak between 3 and 4 V is often observed. Note the break in the n dependence of the oscillation amplitude of the spectrum B_2 at the upper-end gap (10 eV).

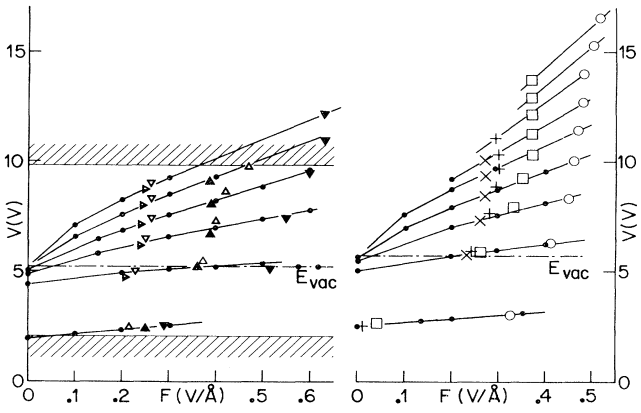

FIG. 3. Peak positions of dI/dV vs V tunnel spectra. Full dots, $E_n(F)$ obtained from numerical integration of the Schrödinger equation by introducing into the Hamiltonian the field potential Fz; other symbols, experiments. Left panel, clean Ni; right panel, oxygen-covered Ni, $c(2\times2)$ and disordered (empty circles). The solid lines are drawn as a guide to the eye. The hatched area denotes the Ni(100) projected bulk band structure (see Ref. 3).

which adjusts the tip-substrate separation to constant tunnel current. The measurements were taken mostly with "blunt" tips of radius of curvature exceeding 20 Å. The well-ordered surfaces exhibited large, atomically flat terraces with well-defined step lines, and sharp LEED spots. The gross features of their spectra appear quite universal: a weakly structured low-voltage region and a strongly and regularly structured high-voltage region. In the following, we concentrate on the Ni spectra.

The clean Ni(100) surface was prepared by Ar sputtering at 500 V for 5 to 10 min and annealing at 600 °C. Since, at fixed tip position and/or higher temperatures, the surface becomes locally unstable, the tunnel spectra were taken at 70 °C, and while scanning. The well-ordered $c(2\times2)$ surface was obtained by annealing at 300 °C after oxygen exposure of 25 L [1 L (langmuir) $=10^{-6}$ Torr·s]; the measurements were taken at 300 °C. The unannealed oxygen-covered surfaces were atomically rough and not terraced, and only diffuse $p(2\times2)$ and $c(2\times2)$ LEED spots were observed.

In Fig. 3, we show the peak positions for various spectra. The electric fields, F, were calculated from curves of tip displacement versus voltage taken simultaneously with the spectra. The peak positions and their dependence on the tip bias field can be understood in terms of a relatively simple model. The peak positions of the tunneling data correspond quite closely to the eigenenergies of the model described in Refs. 1 and 7, extended to include a uniform electric field. The model is a one-dimensional single-particle Schrödinger equation in which the electron is confined by the image (and field) potential in one direction and in the opposite direction by the energy gap of the two-plane-wave description of the substrate. The model contains a single parameter, the width of the dipole-layer region containing the image plane. The data are very well accounted for when this parameter is taken to be n dependent, but field independent. This is consistent with non-free-electron motion along the surface playing an essential role in the binding of these states, and supports the view that surface corrugation is the important source of non-free-electron behavior.[7] The n dependence of our single parameter is given in Table I in the form of $E_{n,\mathrm{corr}}$, the change in the zero-field limit of each image-state energy caused by a change of the dipole-layer-width parameter from its known[2] value of 2.1 Å to a value giving the observed field dependence of each image-state energy. In our view, the entire field evolution can be fitted with a single parameter, i.e., with a field-independent $E_{n,\mathrm{corr}}$, because the spatial region in which the field acts is well characterized by a Hamiltonian depending on z alone. In other words, $E_{n,\mathrm{corr}}$ comes from the atomic potential plus the image near the atomic positions where image and crystal fields are at least an order of magnitude higher than the applied field. The wave function in this region therefore depends only on the energy. Thus, the energy at a particular field value implies its field derivative, that is, the energy at nearby field

TABLE I. Zero-field values of binding energies, E_n, reference binding energies, ϵ_n, and corrugation energies, $E_{n,\mathrm{corr}} = E_n - \epsilon_n$.

	Clean Ni(100)			Oxygen-covered
n	E_n	ϵ_n	$E_{n,\mathrm{corr}}$	E_n
1	−3.25	−2.40	−0.85	−3.2
2	−0.85	−0.33	−0.52	−0.70
3	−0.365	−0.125	−0.24	−0.24
4	−0.18	−0.065	−0.12	−0.11
5	−0.10	−0.040	−0.06	

values. By iteration of this argument, we see that the entire field evolution of the image-state energy $E_n(F)$ is determined by its value at any particular field. The principal role of our model in constructing $E_n(F)$ is to provide the extremely sensitive dependence of the field-sensitive portion of the wave function on the energy. (Note that the approximations underlying this argument improve with decreasing field.) Note that ϵ_n, on the other hand, can be described by a single quantum-defect parameter $\epsilon_n = 0.85/(n-0.39)^2$ eV. In order to describe the spectra of oxygen-covered Ni with an energy-dependent but field-independent parameter, we have to shift the vacuum level upwards by 0.5 ± 0.2 eV. This is consistent with the increase of the Ni work function with oxygen coverage.[15] Since we do not know the dipole-width parameter for the oxygen-covered surface, we cannot calculate ϵ_n and thus $E_{n,\mathrm{corr}}$.

The precision with which the tunneling data determine the values of $E_{n,\mathrm{corr}}$ in Table I illustrates an interesting new potential for tunneling spectroscopy. This precision stems from the very strong dependence of the spatial extent of the image-state wave function on the binding energy. For example, changing the binding energy of the $n=5$ hydrogenic level by only 0.05 eV changes the energy position at which the same state is observed in a field of ~ 0.3 V/Å by ~ 1 eV. Therefore the $E_n(F=0)$ of the higher states are determined within an energy range of 0.02 eV for the present experimental uncertainties at fields ≥ 0.25 V/cm. A simple summary is that the field converts the large quotient of spatial extent to energy range characteristic of the hydrogenic spectrum into a large ratio of energy range to spatial extent. The importance of this effect lies in the potential of the STM for resolution of subtle surface effects contained in the details of the tunneling spectrum, like energies, amplitudes, and line shapes, which are not accessible to other spectroscopies. Note, for example, the shift of the levels shown in Fig. 3 (for a common field value) caused by exposure of the Ni surface to oxygen. Note also the change in line shape and amplitude of the tunneling

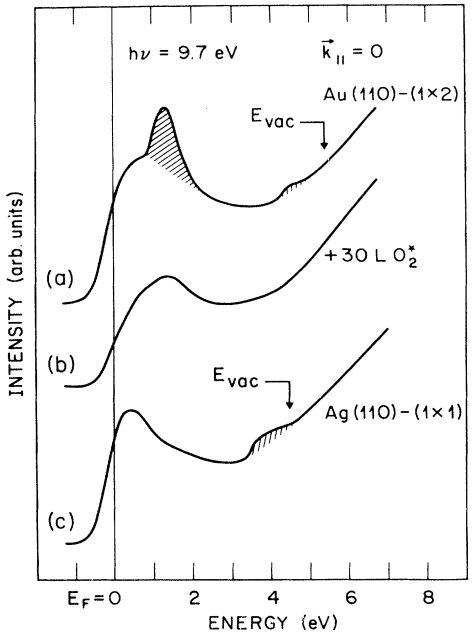

FIG. 4. Normal-incidence inverse-photoemission spectra of (a) clean Au(110)-(1×2); (b) plus 30 L of activated oxygen (O_2); and (c) clean Ag(110)-(1×1). Note the image-state features at E_{vac} (indicated with arrows after Ref. 16) on the clean surfaces in (a) and (c) and the peak at $E_F + 1.3$ eV in (a) only. They are all quenched by oxygen exposure (b). For experimental details of KRIPES see Ref. 6.

spectra in Fig. 2 for ordered and disordered oxygen-covered Ni.

We want to stress that the electronic surface states, which give rise to the oscillatory behavior of the dI/dV (or to features in inverse photoemission), also exist in regions where there is no directional gap. All that matters is that the amplitude of the wave function at and outside the surface is enhanced at a given energy level (resonant surface image states), or the whole wave function is built up at and outside the surface (pure image states). These states contribute to the tunnel current in spite of their quasi two-dimensional character. The resonant state has a propagating component in the bulk. The pure image state has a width and can also decay to the bulk levels as is clearly pointed out by Echenique and Pendry.[1] Therefore, having a gap or not is just a matter of amplitude in the oscillations of dI/dV but not of their existence.

Inverse photoemission complements the description of image states provided by tunneling in two ways. Firstly, the binding energies observed in photoemission are the zero-field limit of the tunneling data. Quantitatively, the zero-field energies of Fig. 3 and Table I agree very well with the $n=1$ and $n \geq 2$ binding energies observed by Johnson and Smith[3] for Ni(100) using inverse photoemission. Figure 4 gives

new KRIPES data showing clearly the $n = 1$ and $n \geq 2$ image states for the 1×2 reconstructed Au(110) surface, and the $n \geq 2$ image states for the Ag(110) surface. The energy positions of all three peaks correspond qualitatively to the zero-field limit of the Ni tunneling data of Fig. 3. Note that the extrapolation of the tunneling data to zero field utilizes the one-dimensional model of Ref. 7 in a nontrivial way. Secondly, photoemission measures directly deviations from free-electron propagation along the surface in the form of the effective mass m^*. For example, the observed angle independence of the binding energy (not shown) for the $n = 1$ state on the Au(110)-(1×2) surface indicates a large effective mass ($m^*/m >> 1$), consistent with its strong reconstruction.[7] KRIPES also indicates a smaller m^* for the $n > 1$ states, consistent with both their greater distance from the surface and the corrugation energies deduced from tunneling data.

We are happy to acknowledge numerous helpful discussions with A. Baratoff, J. Soler, and E. Stoll.

[1]N. Garcia and J. Solana, Surf. Sci. **36**, 262 (1973); P. M. Echenique and J. R. Pendry, J. Phys. C **11**, 2065 (1978).

[2]E. G. McRae, Rev. Mod. Phys. **51**, 541 (1979).

[3]P. D. Johnson and N. V. Smith, Phys. Rev. B **27**, 2527 (1983).

[4]V. Dose, W. Altmann, A. Goldmann, U. Kolac, and J. Rogozik, Phys. Rev. Lett. **52**, 1919 (1984).

[5]D. Straub and F. J. Himpsel, Phys. Rev. Lett. **52**, 1922 (1984).

[6]B. Reihl, K. H. Frank, and R. R. Schlittler, Phys. Rev. B **30**, 7328 (1984).

[7]N. Garcia, B. Reihl, K. H. Frank, and A. R. Williams, Phys. Rev. Lett. **54**, 591 (1985); G. Binnig, N. Garcia, H. Rohrer, J. M. Soler, and F. Flores, Phys. Rev. B **30**, 4816 (1984).

[8]A. J. Jason, Phys. Rev. **156**, 266 (1967). We thank F. Forstmann for pointing out this reference.

[9]K. H. Gundlach, Solid State Electron. **9**, 949 (1966).

[10]J. Maserjian and N. Zamani, J. Appl. Phys. **53**, 559 (1982).

[11]B. T. Jonker, N. C. Bartelt, and R. L. Pakr, Surf. Sci. **127**, 183 (1983).

[12]G. Binnig and H. Rohrer, Helv. Phys. Acta **55**, 726 (1982). Note that in this reference the polarity is given incorrectly.

[13]G. Binnig, H. Rohrer, Ch. Gerber, and E. Weibel, Phys. Rev. Lett. **49**, 57 (1982), and **50**, 120 (1983).

[14]For a review of the technique and references, see G. Binnig and H. Rohrer, Physica (Amsterdam) **127B**, 37 (1984).

[15]D. E. Eastmann and J. K. Cashion, Phys. Rev. Lett. **27**, 1520 (1971); A. R. Kortan and R. L. Park, Phys. Rev. B **23**, 6340 (1981).

[16]H. C. Potter and J. M. Blakely, J. Vac. Sci. Technol. **12**, 635 (1975); A. W. Dweydari and C. H. B. Mee, Phys. Status Solidi a **27**, 223 (1975).